

A quantum computing concept for 1-D elastic wave simulation

Malte Schade,^{1,†} Cyril Bösch,^{1,†} Václav Hapla,¹ Andreas Fichtner¹

¹ Department of Earth and Planetary Sciences, ETH Zurich, Sonneggstrasse 5, 8092 Zurich, Switzerland. Email: cyrill.boesch@erdw.ethz.ch

† These authors contributed equally.

22 December 2023

SUMMARY

Quantum computing has attracted considerable attention in recent years because it promises speed-ups that conventional supercomputers cannot offer, at least for some applications. Though existing quantum computers are, in most cases, still too small to solve significant problems, their future impact on domain sciences is already being explored now. Within this context, we present a quantum computing concept for 1-D elastic wave propagation in heterogeneous media with two components: a theoretical formulation and an implementation on a real quantum computer. The method rests on a finite-difference approximation, followed by a sparsity-preserving transformation of the discrete elastic wave equation to a Schrödinger equation, which can be simulated directly on a gate-based quantum computer. An implementation on an error-free quantum simulator verifies our approach and forms the basis of numerical experiments with small problems on the real quantum computer IBM Brisbane. The latter produce simulation results that qualitatively agree with the error-free version but are contaminated by quantum decoherence and noise effects. Complementing the discrete transformation to the Schrödinger equation by a continuous version allows the replacement of finite differences by other spatial discretisation schemes, such as the spectral-element method. Anticipating the emergence of error-corrected quantum chips, an analogy between our method and analyses of coupled mass-spring systems suggests that our quantum computing approach may lead to wave field simulations that run exponentially faster than simulations on classical computers.

Key words: Numerical modelling, Computational seismology, Theoretical seismology, Wave propagation, Quantum computing

1 INTRODUCTION

The progress of seismological research has always been closely linked to advances in computer technology. As early as 1968, the then-novel IBM 360/65 enabled the random sampling of more than 200,000 seismic models per hour, leading to one of the first Monte Carlo inversions for whole-Earth structure (Press, 1968). The Connection Machine CM-5 was the workhorse for large-scale finite-difference wave field simulations (Igel et al., 1995) and early 2-D acoustic full-waveform inversion (Igel et al., 1996), which could be extended to massive 3-D elastic inversions when GPUs became available (e.g., Bozdağ et al., 2016). Novel chip designs that integrate CPUs and GPUs substantially reduce code complexity, thereby facilitating the efficient development and execution of seismic applications on personal computers (Gebraad and Fichtner, 2023). The list of prominent examples is endless.

Emerging quantum computers (QCs) are opening a new chapter in scientific computing, even though available QCs are still relatively small and inefficient compared to the latest supercomputers that are based on large numbers of CPUs and GPUs. The current stage of the QC development is called *Noisy Intermediate Scale Quantum* (NISQ; coined by Preskill, 2018), since their efficiency is mainly hampered by elevated noise (e.g., Knill, 2005; Nielsen and Chuang, 2010; Preskill, 2018). Recent advances in quantum error correction (e.g., Sivak et al., 2023; Kim et al., 2023; Bravyi et al., 2023) and the design of larger, more modular QCs (e.g., Gibney, 2019; Gambetta, 2020; Sevilla and Riedel, 2020) are promising developments, suggesting the feasibility of quantum computation for numerous algorithmic challenges within the next decade. Presently, QCs are already available in cloud environments, like IBM Quantum, and can be accessed freely for experimental use. This accessibility facilitates the testing and validation of novel quantum algorithms.

QCs harness quantum phenomena such as entanglement and superposition for problem-solving algorithms, thereby promising up to exponential reductions in both runtime and memory usage compared to some classical algorithms (e.g., Nielsen and Chuang, 2010; Benenti et al., 2004). As a result, quantum computation could make it feasible to tackle classes and sizes of problems considered intractable on

traditional computing hardware (e.g., Shor, 1994; Harrow et al., 2009; Montanaro, 2016). Recent studies have started to explore quantum computing to address geophysical problems by proposing quantum simulation algorithms for solving the acoustic wave and Maxwell's equations (e.g., Moradi et al., 2018, 2019; Suau et al., 2021; Jin et al., 2022, 2023). In a broad sense, seismic imaging and related uncertainty quantification problems continue to be primarily limited by computational resources. It is, therefore, timely to assess the potential of quantum computing for the simulation of seismic wave propagation in heterogeneous media, despite the immaturity of the existing QCAs.

This study is intended to be an early step in this direction. We show how elastic wave propagation in heterogeneous media can be simulated using a QC and perform initial experiments on actual QCAs. More specifically, we extend numerical wave propagation via Hamiltonian simulation (Costa et al., 2019; Suau et al., 2021) to heterogeneous media. For this, we employ an analytical Cholesky decomposition, which facilitates the transformation of the elastic wave equation with heterogeneous medium properties to a Schrödinger equation. While we employ a finite-difference approximation of the elastic wave equation, we also discuss the general continuous case and how other numerical methods can be applied. We proceed with the implementation of our method on the QC IBM Brisbane, in order to solve a small-scale problem and explain current challenges. These include systematic errors caused by noise and decoherence rates, which are characteristic for current NISQ QCAs. Anticipating future developments, we finally delve into the potential scalability of an optimal Hamiltonian simulation algorithm on future quantum hardware equipped with error correction. By mapping our problem to a mass-spring model analysed in Babbush et al. (2023), we establish that the algorithm is capable of providing exponential speedup compared to computations on classical computers.

2 A BRIEF SUMMARY OF QUANTUM COMPUTING

To set the stage, we begin with a condensed review of the tensor product formalism and the quantum circuit model that should be accessible to a geophysical audience. This framework is inherently dictated by the postulates of quantum mechanics and forms the fundamental programming model of quantum computing. A more general formalism of density matrices, as well as more in-depth introductions, can be found in the literature (Nielsen and Chuang (2010); Watrous (2018); Adedoyin et al. (2022)).

2.1 Quantum particles and state space

Consider a single quantum particle characterised by its quantised properties, such as the atomic energy level. This particle can occupy N different orthogonal basis states, which span the state space of the particle. To the basis states, we assign labels $\Sigma = \{0, \dots, N-1\}$, collectively referred to as the label set of size $|\Sigma| = N$. A particle with N basis states is called an N -level particle. The current state of the observable is represented by the state vector $|\psi\rangle = [\alpha_0, \dots, \alpha_{N-1}]^T \in \mathbb{C}^N$, where $\alpha_k \in \mathbb{C}$ is the probability amplitude corresponding to the k -th basis state $|k\rangle$, written in the bra-ket or Dirac notation that is ubiquitous in quantum mechanics. It encapsulates all information about the individual particles and their number and concisely represents exponentially large state vectors. The ket $|a\rangle$ is a column vector, whereas the bra $\langle b|$ is a row vector with complex conjugate transpose $\langle b|^\dagger = |b\rangle$. Bra and ket form the bra-ket $\langle b|a\rangle$, which is the scalar product $|b\rangle^\dagger \cdot |a\rangle$. The main difference, compared to the common vector notation in linear algebra, is that the content of the bra/ket does not represent individual vector entries but some convenient collective label. The state vector $|\psi\rangle$ can be expressed in terms of the basis states $|k\rangle$ with $k = 0, \dots, N-1$ as the linear combination $|\psi\rangle = [\alpha_0, \dots, \alpha_{N-1}]^T = \alpha_0|0\rangle + \alpha_1|1\rangle + \dots + \alpha_{N-1}|N-1\rangle \in \mathbb{C}^N$, which is called a superposition state.

The state vector of a system composed of n particles is given by

$$|\psi\rangle = |\psi_0\rangle \otimes |\psi_1\rangle \cdots \otimes |\psi_{n-1}\rangle = \bigotimes_{j=0}^{n-1} |\psi_j\rangle \in \mathbb{C}^N, \quad N = N_0 N_1 \dots N_{n-1} = \prod_{j=0}^{n-1} N_j, \quad (1)$$

where $|\psi_j\rangle \in \mathbb{C}^{N_j}$ is the state of the j^{th} particle, and N_j is the number of states that it can occupy. We reuse the symbols N and ψ , because a single-particle system is a special case of a multi-particle system. The symbol \otimes denotes the Kronecker or tensor product. For two arbitrary states \mathbf{u} and \mathbf{v} , it is defined as

$$\mathbf{u} \otimes \mathbf{v} = \begin{bmatrix} u_0 \mathbf{v} \\ \vdots \\ u_{N_{\mathbf{u}}-1} \mathbf{v} \end{bmatrix} \in \mathbb{C}^{N_{\mathbf{u}} N_{\mathbf{v}}}, \quad (2)$$

where $N_{\mathbf{u}}$ and $N_{\mathbf{v}}$ are the lengths of the vectors \mathbf{u} and \mathbf{v} , respectively. Now, we introduce the kets with integer strings. If we assume basis vectors $|j\rangle$ and $|k\rangle$ having label sets Σ and Γ , respectively, we have

$$|j\rangle \otimes |k\rangle = |jk\rangle, \quad (3)$$

where jk is a string representing $(j, k) \in \Sigma \times \Gamma$ with the index $I = j \cdot |\Gamma| + k$ in the alphabetical ordering of $\Sigma \times \Gamma$, and $|jk\rangle$ is a vector with 1 at the I^{th} position and zeros otherwise. The tensor product of two or more superposition states can be deduced from (3) using multi-linearity.

Quantum computing typically uses particles with two basis states, which is a natural choice because it is the minimum number for a non-trivial system and the easiest to distinguish and manipulate in a hardware implementation. Such a particle is referred to as a qubit in analogy to the classical bit. Just like a bit, a qubit is an abstract object that can be mapped to a concrete physical object in many different ways. The two standard basis states $|0\rangle = [1, 0]^T$ and $|1\rangle = [0, 1]^T$ can be represented, for instance, by the spin-up and spin-down of a spinor or

two disjoint subsets of atomic energy levels. A single qubit $|\psi\rangle$ can be in an arbitrary superposition of the two states, $|\psi\rangle = \beta_0|0\rangle + \beta_1|1\rangle = [\beta_0, \beta_1]^T \in \mathbb{C}^2$, in contrast to a classical bit, which can only be in either of two states, 0 or 1. A state of an n -qubit system with qubits $|\psi_j\rangle$, $j = 0, \dots, n-1$, is again given by (1) with $N = 2^n$, because $N_j = 2$ for every qubit. We can see that the quantum state space dimension N grows exponentially with the number of qubits n . This is the main source of the quantum computing potential.

Any quantum state must be normalised, i.e., satisfy the normalisation condition

$$\| |\psi\rangle \| = \sum_{k=0}^{N-1} |\alpha_k|^2 = 1. \quad (4)$$

Combining normalised states with the \otimes product, the resulting composite state is normalised as well. If $\alpha_k \neq 0$ for at least two different indices k , then the state $|\psi\rangle$ simultaneously holds multiple potential outcomes $\Omega = \{|k\rangle : \alpha_k \neq 0\}$ and is called a superposition state. In contrast to classical systems, a measurement of the quantum system causes the state $|\psi\rangle$ to collapse from the superposition into one of the possible basis states $|k\rangle \in \Omega$ randomly with probability $P(k) = |\alpha_k|^2$, which explains the term probability amplitude used for the coefficients α_k . The type of measurement just introduced is a full-system measurement in the standard basis, which is the simplest case; we do not deal with more general cases, which can be found in the literature at the top of this section. Measurements allow us to read the label of the collapsed state in the form of classical bits, forming the only interface between quantum and classical information.

2.2 Quantum gates and circuits

Quantum computations consist of reversible, information-preserving transformations, represented by matrices \mathbf{U} that are unitary, i.e., that satisfy $\mathbf{U}^{-1} = \mathbf{U}^\dagger$, where \dagger represents a conjugate transpose. A gate-based QC implements a set of gates, which are hardware implementations of unitary operations forming a quantum-Turing complete set. These operations can simulate an arbitrary quantum algorithm, given a sufficient time and number of qubits. The only non-unitary QC operation is the measurement.

In practical quantum programming, a somewhat larger, redundant set of quantum gates is used for more convenient programming but then automatically translated into the minimum set supported by the hardware as needed before execution. These basic gates form the “quantum assembly language”. They include single-qubit gates of size 2×2 such as the identity gate \mathbf{G}_I , the Hadamard gate \mathbf{G}_H , the NOT gate \mathbf{G}_X or rotation gates, and multi-qubit gates such as \mathbf{G}_{CNOT} , $\mathbf{G}_{SWAP} \in \mathbb{C}^{4 \times 4}$ or the Toffoli gate $\mathbf{G}_{CCNOT} \in \mathbb{C}^{8 \times 8}$.

Any quantum algorithm is formed by a combination of basic gates (possibly used repeatedly) that are composed into a quantum circuit, represented by a unitary matrix \mathbf{W} formed by a product of D layers \mathbf{W}_j ,

$$\mathbf{W} = \mathbf{W}_{D-1} \mathbf{W}_{D-2} \dots \mathbf{W}_0 = \prod_{j=D-1}^0 \mathbf{W}_j \in \mathbb{C}^{N \times N}, \quad (5)$$

where D is called the circuit depth. The layers are evaluated from right to left in time, meaning that the indices reflect the order of evaluation. Further, each layer \mathbf{W}_j is formed by a tensor product of basic gates,

$$\mathbf{W}_j = \mathbf{G}_{j,t_0} \otimes \mathbf{G}_{j,t_1} \otimes \dots \otimes \mathbf{G}_{j,t_i} \otimes \dots \in \mathbb{C}^{N \times N}, \quad (6)$$

where $t_i \in \{I, H, X, CNOT, \dots\}$ is the type of the (basic) gate and \otimes is the extension of the Kronecker product from (2) to arbitrary matrices $\mathbf{A} \in \mathbb{C}^{M_A \times N_A}$ with entries denoted as $a_{i,j}$, and $\mathbf{B} \in \mathbb{C}^{M_B \times N_B}$ as

$$\mathbf{A} \otimes \mathbf{B} = \begin{bmatrix} a_{0,0}\mathbf{B} & \dots & a_{0,N_A-1}\mathbf{B} \\ \vdots & \ddots & \vdots \\ a_{M_A-1,0}\mathbf{B} & \dots & a_{M_A-1,N_A-1}\mathbf{B} \end{bmatrix} \in \mathbb{C}^{M_A M_B \times N_A N_B}. \quad (7)$$

The number of factors in the tensor multi-product (6) is at most n (n if every basic gate of the layer acts on a single qubit), but it can vary between layers based on the basic gates used; the only requirement is that the total size is N so that (5) makes sense. The art of finding the most efficient circuit for the given task, i.e., the representation with the lowest n and D , is a subject of today’s research in quantum computing.

2.3 Hamiltonian simulation

The dynamics of any quantum system are governed by the Schrödinger equation

$$i\partial_t |\psi\rangle = \mathbf{H} |\psi\rangle, \quad (8)$$

where i denotes the imaginary unit, and $\mathbf{H} \in \mathbb{C}^{N \times N}$ is a Hermitian linear operator, called the Hamiltonian, which controls the time evolution of the system. The solution of (8) can symbolically be written using the matrix exponential,

$$|\psi(t)\rangle = e^{-i\mathbf{H}t} |\psi(0)\rangle, \quad (9)$$

with the initial state $|\psi(0)\rangle$. The time evolution operator $\mathbf{U}(t) = \exp(-i\mathbf{H}t)$ is unitary. Our approach to elastic wave propagation on a QC rests on the quantum or Hamiltonian simulation (HS) approach (e.g., Georgescu et al., 2014; Nielsen and Chuang, 2010), which amounts to the direct evaluation of (9). HS was originally introduced to model multi-particle quantum dynamic systems using QCs. Due to the

aforementioned exponential space growth, quantum dynamics modelling becomes prohibitively complex on classical computers. In contrast, by being quantum systems themselves, QCs naturally feature the same state space expansion, potentially making multi-particle simulations possible.

For initialisation, HS requires the application of a unitary operation \mathbf{V} that sets the desired initial state, i.e. $|\psi(0)\rangle = \mathbf{V}|00..00\rangle$. Subsequently, the unitary time evolution operator $\mathbf{U}(t)$, constructed using basic gates, is applied to $|\psi(0)\rangle$,

$$|\psi(t)\rangle = \mathbf{U}(t)|\psi(0)\rangle. \quad (10)$$

The main challenge of HS is that the matrix exponential $\mathbf{U}(t) = \exp(-i\mathbf{H}t)$ is notoriously difficult to evaluate explicitly. Hence, the application of $\mathbf{U}(t)$ is replaced by some unitary $\mathbf{U}_A(t)$ that evolves the initial state to the final one with the desired error ε , $\|\mathbf{U}(t)|\psi(0)\rangle - \mathbf{U}_A(t)|\psi(0)\rangle\| < \varepsilon$, and can be implemented efficiently using basic quantum gates, with circuit depth growing along with $1/\varepsilon$.

Since the matrix exponential can be expressed in terms of a Taylor series, $\mathbf{U}(t) = e^{-i\mathbf{H}t} = \sum_{k=0}^{\infty} \frac{(-i\mathbf{H}t)^k}{k!}$, we can approximate it by truncating it to a finite Taylor sum, $\mathbf{U}_A(t) = \sum_{k=0}^{m-1} \frac{(-i\mathbf{H}t)^k}{k!} \approx e^{-i\mathbf{H}t}$, with some integer $m < \infty$. The finite sum is then further approximated by decomposing \mathbf{H} into a sum of unitary matrices. The number of terms in this sum, determined by the given \mathbf{H} and desired accuracy, dictates the efficiency of this particular approach (Berry et al., 2015).

Other approaches can be found in the literature, with efficiency varying based on properties of the given \mathbf{H} . These include methods based on the Trotter-Suzuki Decomposition (e.g., Trotter, 1959; Suzuki, 1976, 1991; Hatano and Suzuki, 2005; Dhand and Sanders, 2014; Yi and Crosson, 2022) and the recent qubitisation approach (Low and Chuang, 2019), discussed more in detail in appendix B.

It has been shown that HS can achieve up to exponential speedup compared to analogous classical algorithms (e.g., Berry et al., 2007; Childs et al., 2018; Daley et al., 2022; Babbush et al., 2023). We will discuss this matter as well as the question of utilising the final state in section 5.

In addition to the simulation of quantum systems, HS may also be harnessed to solve classical equations of motion, provided that an invertible transformation to the Schrödinger equation can be found (e.g., Costa et al., 2019; Suau et al., 2021; Babbush et al., 2023). Such transformations exist for classical wave equations (Süsstrunk and Huber, 2016), which share key properties with the Schrödinger equation. Both describe wave-like phenomena and are linear. In the following, we will describe such a transformation for the elastic wave equation with heterogeneous medium parameters.

3 ELASTIC WAVEFORM PROPAGATION USING HS

We consider a 1-D elastic wave equation in the spatial domain $x \in [0, W]$ subject to Dirichlet and Neumann boundary conditions on the right and left, respectively,

$$\rho(x)\partial_{tt}u(x, t) = \partial_x[\mu(x)\partial_x]u(x, t), \quad \partial_xu(0, t) = 0, \quad u(W, t) = 0, \quad (11)$$

with time t , the wave field $u(x, t)$, density $\rho(x)$ and elastic modulus $\mu(x)$. Furthermore, the wave field is subject to the initial conditions $u_0 = u(0, x)$ and $v_0 = \partial_tu(0, x)$. We introduce a first-order finite-difference discretisation in space with 2^{n-1} grid points, each with position and velocity, and a grid spacing of $\Delta x = W/(2^{n-1} - 1)$, thereby approximating the continuous wave field $u(x, t)$ by the discrete wave field vector $\mathbf{u}(t) = [u(x_0, t), \dots, u(x_{2^{n-1}-1}, t)]^T$. In section 5.3, we discuss the potential use of other discretisation methods. We further define the positive definite mass matrix \mathbf{M} that serves as a discrete representation of the density distribution,

$$\mathbf{M} = \begin{bmatrix} \rho(x_0) & 0 & \dots & 0 \\ 0 & \rho(x_1) & \dots & 0 \\ \vdots & \vdots & \ddots & \vdots \\ 0 & 0 & \dots & \rho(x_{2^{n-1}-1}) \end{bmatrix}, \quad (12)$$

and the positive definite elasticity matrix \mathbf{E} , which is the discrete version of $\mu(x)$,

$$\mathbf{E} = \begin{bmatrix} \mu(x_0) & 0 & \dots & 0 \\ 0 & \mu(x_1) & \dots & 0 \\ \vdots & \vdots & \ddots & \vdots \\ 0 & 0 & \dots & \mu(x_{2^{n-1}-1}) \end{bmatrix}. \quad (13)$$

To obtain the stiffness matrix \mathbf{K} , we use a second-order stencil with the stress given by $\sigma_i = \mu(x_i)[u(x_{i+1}) - u(x_i)]/\Delta x$ and the elastic forces by $\partial_x\sigma(x_i) = [\sigma(x_i) - \sigma(x_{i-1})]/\Delta x$ (e.g., Moczo et al., 2014). We define the first-order accurate forward finite-difference matrix \mathbf{D} as

$$\mathbf{D} = \frac{1}{\Delta x} \begin{bmatrix} -1 & 1 & 0 & \dots & 0 \\ 0 & -1 & 1 & \dots & 0 \\ 0 & 0 & -1 & \dots & 0 \\ \vdots & \vdots & \vdots & \ddots & \vdots \\ 0 & 0 & 0 & \dots & -1 \end{bmatrix}. \quad (14)$$

The symmetric negative-definite stiffness matrix \mathbf{K} is consequently obtained as

$$\mathbf{K} = -\mathbf{D}^T \mathbf{E} \mathbf{D}. \quad (15)$$

This implementation naturally results in a Dirichlet and a Neumann boundary condition on the right and left, respectively, assuming two ghost nodes. In the interest of a smooth derivation, we defer the case of arbitrary boundary conditions to appendix C. With these definitions, the space-discretised wave equation reads

$$\mathbf{M} \partial_{tt} \mathbf{u} = \mathbf{K} \mathbf{u}. \quad (16)$$

To solve (16) on a QC, it needs to be transformed into the Schrödinger equation (8). For this, we first apply a transformation that utilises the positive definite, diagonal square root matrix $\mathbf{M}^{1/2}$, which produces the mass-transformed wave field $\tilde{\mathbf{u}} = \mathbf{M}^{1/2} \mathbf{u}$ and the mass-transformed stiffness matrix $\tilde{\mathbf{K}} = \mathbf{M}^{-1/2} \mathbf{K} \mathbf{M}^{-1/2}$. The latter inherits the property of being symmetric negative-definite from \mathbf{K} . We proceed by transforming the second-order system into a first-order system

$$\partial_t \begin{bmatrix} \tilde{\mathbf{u}} \\ \tilde{\mathbf{v}} \end{bmatrix} = \begin{bmatrix} \mathbf{0} & \mathbb{1}_{2^{n-1} \times 2^{n-1}} \\ \tilde{\mathbf{K}} & \mathbf{0} \end{bmatrix} \begin{bmatrix} \tilde{\mathbf{u}} \\ \tilde{\mathbf{v}} \end{bmatrix} = \mathbf{Q} \begin{bmatrix} \tilde{\mathbf{u}} \\ \tilde{\mathbf{v}} \end{bmatrix}, \quad (17)$$

where $\tilde{\mathbf{v}} = \partial_t \tilde{\mathbf{u}} = \mathbf{M}^{1/2} \partial_t \mathbf{u} \in \mathbb{R}^{2^{n-1}}$ is the mass-transformed velocity vector and \mathbf{Q} the impedance matrix. While (17) is already closer to the Schrödinger equation than (16), it remains to symmetrise \mathbf{Q} and obtain the imaginary unit i on the left-hand side. For this, we multiply (17) by an arbitrary invertible transformation $\mathbf{T} \in \mathbb{R}^{2^n \times 2^n}$, which results in

$$\partial_t \mathbf{T} \begin{bmatrix} \tilde{\mathbf{u}} \\ \tilde{\mathbf{v}} \end{bmatrix} = \mathbf{T} \mathbf{Q} \mathbf{T}^{-1} \mathbf{T} \begin{bmatrix} \tilde{\mathbf{u}} \\ \tilde{\mathbf{v}} \end{bmatrix}. \quad (18)$$

If \mathbf{T} can be constructed such that $\mathbf{H} = i \mathbf{T} \mathbf{Q} \mathbf{T}^{-1}$ is Hermitian, we can employ \mathbf{H} as a quantum Hamiltonian that emulates elastic wave field dynamics. The transformed wave field vector is identified as $|\Phi\rangle = \mathbf{T}[\tilde{\mathbf{u}}, \tilde{\mathbf{v}}]^T$, which is subsequently encoded in a quantum state. The final Schrödinger equation for 1-D elastic wave propagation therefore becomes

$$i |\Phi(t)\rangle = \mathbf{H} |\Phi(t)\rangle, \quad (19)$$

subject to the initial conditions

$$|\Phi(0)\rangle = \mathbf{T} \begin{bmatrix} \mathbf{M}^{1/2} \mathbf{u}_0 \\ \mathbf{M}^{1/2} \mathbf{v}_0 \end{bmatrix}, \quad (20)$$

which are typically sparse in seismic applications thanks to the spatial localisation of sources. Furthermore, owing to the localised interactions of the discretised degrees of freedom, both the mass and stiffness matrices are sparse, which implies that \mathbf{Q} is sparse, too. Eq. (19) can, in principle, be solved by a QC, and it is isomorphic to the discretised elastic wave equation (16) because \mathbf{T} is invertible. The actual elastic wave field at all times can, therefore, be reconstructed via

$$[\tilde{\mathbf{u}}(t), \tilde{\mathbf{v}}(t)]^T = \mathbf{T}^{-1} |\Phi(t)\rangle \quad \text{and} \quad \mathbf{u}(t) = \mathbf{M}^{-1/2} \tilde{\mathbf{u}}(t). \quad (21)$$

It remains to design a practically useful transformation \mathbf{T} . Several transformations exist that achieve this classical-to-quantum mapping (e.g., Süsstrunk and Huber, 2016; Kane and Lubensky, 2014; Babbush et al., 2023). In the subsequent analysis, we choose a transformation that retains sparsity in both the initial conditions (20) and the Hamiltonian \mathbf{H} . This preservation of sparsity is pivotal for scalable HS algorithms. We will revisit this topic in appendix B. To construct the desired \mathbf{T} , we define

$$\mathbf{U} = \mathbf{E}^{1/2} \mathbf{D} \mathbf{M}^{-1/2}, \quad (22)$$

such that

$$\tilde{\mathbf{K}} = -\mathbf{U}^T \mathbf{U} = -\mathbf{M}^{-1/2} \mathbf{D}^T \mathbf{E} \mathbf{D} \mathbf{M}^{-1/2}, \quad (23)$$

which is an analytical Cholesky decomposition, with \mathbf{U} being the upper triangular matrix. Since the negative-definite $\tilde{\mathbf{K}}$ is invertible, \mathbf{U} is also invertible. This follows from $\det(\tilde{\mathbf{K}}) = \det(-\mathbf{U}^T \mathbf{U}) = \det(-\mathbf{U}^T) \det(\mathbf{U})$. With this, we finally define

$$\mathbf{T} = \begin{bmatrix} \mathbf{U} & \mathbf{0} \\ \mathbf{0} & \mathbb{1}_{2^{n-1} \times 2^{n-1}} \end{bmatrix}, \quad (24)$$

which leads to

$$\mathbf{H} = i \mathbf{T} \mathbf{Q} \mathbf{T}^{-1} = i \begin{bmatrix} \mathbf{U} & \mathbf{0} \\ \mathbf{0} & \mathbb{1}_{2^{n-1} \times 2^{n-1}} \end{bmatrix} \begin{bmatrix} \mathbf{0} & \mathbb{1}_{2^{n-1} \times 2^{n-1}} \\ -\mathbf{U}^T \mathbf{U} & \mathbf{0} \end{bmatrix} \begin{bmatrix} \mathbf{U}^{-1} & \mathbf{0} \\ \mathbf{0} & \mathbb{1}_{2^{n-1} \times 2^{n-1}} \end{bmatrix} = i \begin{bmatrix} \mathbf{0} & \mathbf{U} \\ -\mathbf{U}^T & \mathbf{0} \end{bmatrix}, \quad (25)$$

where \mathbf{H} is Hermitian, meaning that it can be employed as a Hamiltonian in QC simulations. This step concludes the process of mapping the elastic wave equation with heterogeneous medium parameters to the Schrödinger equation. It produces a Hamiltonian with two entries per row (2-sparse) for a finite-difference scheme of second-order accuracy in the 1-D case. We discuss higher space dimensions in section 5.

4 IMPLEMENTATION AND EXPERIMENTS ON QUANTUM SIMULATORS AND COMPUTERS

The transformations discussed in the previous sections are pre-processing steps executed on a classical computer. In the following, we present the implementation of the transformed elastic wave equation on both an actual QC and an ideal (error-free) quantum simulator. A quantum simulator is a software running on classical computers that emulates the behaviour of actual QCs. We create a quantum circuit that defines all operations that must be physically conducted on qubits during the circuit's runtime. All of these operations, except for the measurements of the qubit states, are necessarily unitary. Hence, the quantum circuit itself can be represented by a single unitary matrix.

The quantum circuit that solves the elastic wave equation through quantum time evolution is composed of 3 sub-circuits; (1) one that prepares the initial condition $|\Phi(0)\rangle$, (2) one that performs the quantum simulation through implementing the Hamiltonian \mathbf{H} , and (3) one that utilises the evolved state $|\Phi(t)\rangle$. This utilisation can, for example, be a measurement of the qubits yielding binary results. In this section, we employ the open-source software development kit QISKit by IBM Research (Aleksandrowicz et al., 2019) to create and run the quantum circuit on quantum simulators and actual QCs. The representation of the initial conditions $|\Phi(0)\rangle$ on a QC requires normalisation,

$$|\Phi_{\text{norm}}(0)\rangle = \frac{|\Phi(0)\rangle}{\|\Phi(0)\rangle\|}, \quad (26)$$

because quantum states must have a unit norm. This normalisation has to be undone at the end of the simulation via

$$|\Phi(t)\rangle = |\Phi_{\text{norm}}(t)\rangle \|\Phi(0)\rangle\|. \quad (27)$$

Due to the linearity of (19), no information is lost in this procedure. We begin the simulation procedure with the initialisation of an n -qubit quantum register, $|00..00\rangle = |0\rangle \otimes \dots \otimes |0\rangle \in \mathbb{C}^{2^n}$, using the QISKit constructor `qc = QuantumCircuit(n)`. We must then apply the initialisation unitary transformation \mathbf{V} to obtain the initial state,

$$|\Phi_{\text{norm}}(0)\rangle = \mathbf{V}|00..00\rangle. \quad (28)$$

This is done by the QISKit method `qc.prepare_state(phi0_norm)`. Constructing and applying the quantum circuit corresponding to \mathbf{V} can be challenging (e.g., Kak, 1999). However, in the context of seismic applications and using the above-derived transformation \mathbf{T} , the initial state $|\Phi_{\text{norm}}(0)\rangle$ is sparse and can be initialised efficiently as discussed in appendix B. Next, the quantum wave simulation circuit is realised by appending the time-evolution operator

$$\mathbf{U}(t) = e^{-i\mathbf{H}t}, \quad (29)$$

to the quantum circuit, yielding

$$|\Phi_{\text{norm}}(t)\rangle = \mathbf{U}(t)|\Phi_{\text{norm}}(0)\rangle. \quad (30)$$

We currently perform the time evolution, i.e., the action of \mathbf{U} , using QISKit class `PauliEvolutionGate`. It implements the scaling and squaring method (Al-Mohy and Higham, 2010). We have chosen this method because it is implementable on today's freely accessible QCs, such as IBM Brisbane, with a moderate circuit overhead for small-scale problems. For large-scale problems, which will only become tractable on QCs with higher qubit counts and better error correction, this approach becomes inapplicable due to the exponential scaling; for n qubits, \mathbf{U} is a $2^n \times 2^n$ dense matrix that needs to be stored and applied to $|\Phi_{\text{norm}}(0)\rangle$. As already explained in section 2.3, the action of \mathbf{U} must be carried out only approximately to obtain a scalable approach. Appendix B discusses scaling if the best available approaches are applied to our settings.

Finally, the resulting quantum state $|\Phi(t)\rangle$ is utilised further within the QC or is read out using quantum state tomography (Smolin et al., 2012). Here, we opt for the latter to compare the QC simulation with the solution obtained on a classical computer. However, this becomes prohibitively expensive for large problems. Notably, in situations where the state vectors are strictly real, $|\Phi(t)\rangle$ forms a 2^n -dimensional distribution that needs to be sampled. Additionally, to get a sample, a quantum measurement needs to be performed, which collapses the state (Nielsen and Chuang, 2010), therefore requiring a new full run for each sample. Reading out the final state is then more computationally demanding than the HS itself. We discuss how to circumvent this problem in the context of imaging in section 5. In summary, the quantum time evolution circuit proceeds as follows:

- (i) Initialization of the quantum circuit with the appropriate number of bits, each in $|0\rangle$ state.
- (ii) Preparation of the state corresponding to the initial wave field per (28).
- (iii) Time-evolution (30) via application of the time-evolution operator (29).
- (iv) State tomography via repeated measurement and evaluation.

The quantum state tomography output, $|\Phi_{\text{norm}}(t)\rangle$, represents the quantum state after the simulation. To retrieve the classical wave field, we reverse the normalisation, apply the inverse transform \mathbf{T}^{-1} and subsequently apply $\mathbf{M}^{-1/2}$.

For demonstration, we simulate a 7 grid-point problem, which we found to be the maximum number of grid points realisable on IBM Brisbane. The setup and all results of the numerical experiment are summarised in Fig. 4. We use Dirichlet boundary conditions, a uniform space discretisation dx of 1 m, and monotonically increasing density and elastic modulus distributions.

As the numerical ground truth, we use an ordinary differential equation (ODE) solver based on an explicit Runge-Kutta method (e.g., Dormand and Prince, 1980; Shampine, 1986) to directly integrate (33). Since the quantum formalism is exactly isomorphic to the classical one, the HS should exactly reproduce this solution, including finite-difference errors such as grid dispersion caused by the small number of grid points per wavelength. To investigate the correctness of our quantum implementation, we use an ideal QC simulator, i.e., a quantum

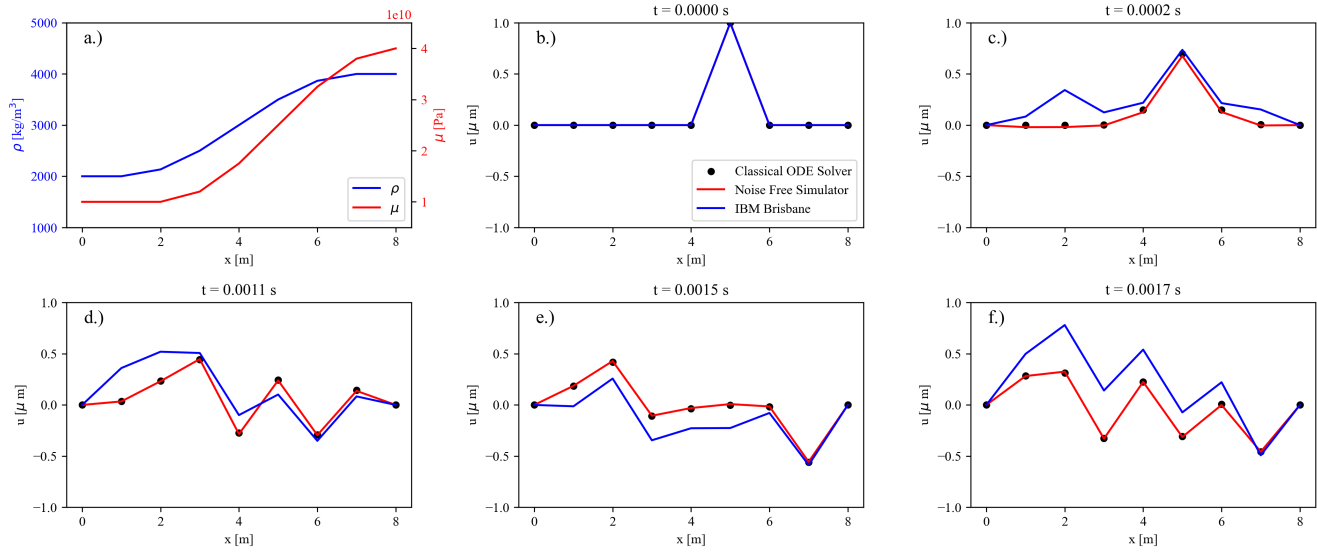


Figure 1. Comparison of elastic wave field simulations using a classical ODE solver (black), an ideal quantum simulator (red), and the quantum computer IBM Brisbane (blue). (a) Heterogeneous distributions of density and elastic modulus. (b-e) wave field at selected times.

simulator that does not imitate quantum noise and decoherence effects of the current-generation QCs but appears as perfectly noise-free. The numerical ground truth agrees with the solution from the simulator. A relative error of 0.01 %, which is not visible in the plot, is attributed to the quantum tomography, as discussed above.

Finally, we solve the problem on the real QC IBM Brisbane. To perform the quantum state tomography extracting the quantum simulation results, we run the whole circuit $10^3 \times 2^n$ times to reduce the relative error contribution of the quantum state tomography to 0.03. We observe qualitative agreement between the numerical ground truth and the simulation on the QC but substantial errors of up to 60 % in the norm of their difference. These can be attributed to the high decoherence and noise rates of real QCs, as opposed to the ideal QC simulator.

When a quantum algorithm is executed, a sequence of quantum gates is applied to each qubit as discussed in section 2. The number of gates applied to the qubits is known as the circuit depth. Each gate application has a certain success rate, the probability that the gate operation is executed correctly. IBM Brisbane's gates have an error per layered gate for a 100-qubit chain (EPLG) of 1.9 %, equaling an approximate average 5-qubit layer success rate of 99.9 % (Gambetta (2020); Collins and Easterly (2021)). For the 7 grid point problem, our implementation yields an average circuit depth of 870 quantum gates with 5 qubits, which results roughly in a probability of $0.999^{870} \approx 0.42$ for a successful execution of the whole circuit. This indeed reflects approximately the error level of 60 % in our simulation. Increasing the number of grid points will increase the circuit depth and hence the error, currently limiting the problem size to 7 grid points.

On today's QCs, the error characteristics vary substantially per hardware and problem. Quantum processing units (QPUs) have different interaction topographies, implemented gate sets, and gate error rates of individual qubits and require continuous re-calibration. Hence, it is expected that different error characteristics would appear if we had chosen a different QC, different qubits within the same QC, or even just a different runtime. Improving the reliability of quantum chips, in combination with more advanced error mitigation methods, is a vivid research field. It is, therefore, expected that substantial improvements will be achieved in the coming years and decades.

5 DISCUSSION

In the following paragraphs, we provide additional details concerning potential computational speed-ups, the utilisation of the final state, a continuous version of the above-described transformations in the context of alternative numerical methods, and future extensions of the 1-D elastic concept.

5.1 Exponential quantum speedup

Identifying the boundary beyond which QCs provide a computational advantage over their classical counterparts for a particular problem is a non-trivial task and subject to intensive theoretical (e.g., Grover, 1996; Shor, 1999; Liu et al., 2021; Gyurik et al., 2022; França and Garcia-Patron, 2022; Hibat-Allah et al., 2023; Babbush et al., 2023) as well as experimental research (e.g., Maslov et al., 2021; Liu et al., 2021; Sanders, 2021; Bulmer et al., 2022; Huang et al., 2022; Madsen et al., 2022). Establishing practical results based on theory largely depends on the anticipated emergence of error-corrected quantum chips, as opposed to today's NISQ machines (Preskill, 2018).

The first promise of quantum computing concerns the storage size. For classical computational methods, the number of bits required

to store the entire wave field scales linearly with the number of grid points. In contrast, for quantum computational methods like the one discussed here, the number of required qubits scales only logarithmically because, reciprocally, the quantum state space grows exponentially with the number of qubits. For instance, assume a discretised wave field with two real-valued parameters per grid point, such as displacement and velocity, and Earth volume $1.083 \times 10^{12} \text{ km}^3$. Representing a full wave field in mm^3 resolution requires merely 101 qubits.

The second promise is runtime speed-up. Building on work by Babbush et al. (2023), we demonstrate in appendix B, that the quantum algorithm presented in sections 2.3–4 has a runtime complexity that is polynomial in n and poly-logarithmic in N , provided that the best currently available approaches are used for the individual simulation steps. In contrast, any classical algorithm necessarily has at least exponential complexity in n and polynomial in N (Babbush et al., 2023). In the foreseeable future, the specific N for which the quantum approach becomes actually faster might be above the limit given by the available hardware. However, the promise is highly enticing in the long term.

5.2 Utilising the final state

As discussed in section 4, reading out the full state with quantum state tomography scales polynomially in N and exponentially in n . Hence, the read-out would nullify the exponential speed-up. Babbush et al. (2023) show that it is possible to read out certain properties, such as kinetic energy or potential energy of a subdomain of the model, in polynomial time, suggesting that the exponential speed-up can be preserved in such cases. A similar logic will be required to preserve the exponential speed-up for seismological purposes, e.g., by computing a misfit function on the fly instead of reading out the complete time evolution of the wave field. This topic will be the subject of a follow-up publication.

5.3 Continuous transformation and the use of other numerical schemes

In section 3, we performed the transformation of the elastic wave equation to the Schrödinger equation in the discrete domain in the interest of conciseness. A conceptually similar transformation can be designed in the continuous domain, thereby enabling the use of alternative numerical methods, including finite-element or spectral-element schemes. Furthermore, the continuous approach illuminates how transformations must be designed to achieve self-adjointness with respect to the natural inner product in quantum physics, loosely referred to as the quantum inner product in the following. To understand this, we consider the wave operator for the 1-D elastic wave equation

$$\mathcal{L} := \partial_x [\mu \partial_x]. \quad (31)$$

We omit the dependence on space, x for brevity. Following the approach in section 3, we define a transformation utilising the square root of density $\rho^{1/2}$, resulting in the density-transformed wave field $\tilde{u} = \rho^{1/2} u$ and a density-transformed wave operator

$$\mathcal{L}_\rho := \rho^{-1/2} \partial_x [\mu \partial_x] \rho^{-1/2}. \quad (32)$$

We then transform the continuous wave equation to a first-order system

$$\partial_t \begin{bmatrix} \tilde{u} \\ \tilde{v} \end{bmatrix} = \begin{bmatrix} 0 & 1 \\ \mathcal{L}_\rho & 0 \end{bmatrix} \begin{bmatrix} \tilde{u} \\ \tilde{v} \end{bmatrix} =: \mathcal{Q} \begin{bmatrix} \tilde{u} \\ \tilde{v} \end{bmatrix}, \quad (33)$$

where $\tilde{v} = \partial_t \tilde{u} = \rho^{1/2} \partial_t u \in \mathbb{R}$ are the density-transformed velocities. We now aim to construct an invertible transformation \mathcal{T} that maps equation (33) to a continuous Schrödinger equation. Mathematically, this means that $H = i\mathcal{T}\mathcal{Q}\mathcal{T}^{-1}$ has to be self-adjoint under the quantum inner product

$$\left\langle \begin{bmatrix} a \\ b \end{bmatrix} \middle| \begin{bmatrix} c \\ d \end{bmatrix} \right\rangle = \langle a, c \rangle + \langle b, d \rangle = \int_0^W dx a^*(x) c(x) + \int_0^W dx b^*(x) d(x). \quad (34)$$

In appendix A, we show that there exists such a transformation which is invertible. The resulting Hamiltonian is given by

$$\mathcal{H} = i \begin{bmatrix} 0 & \mu^{1/2} \partial_x \rho^{-1/2} \\ \rho^{1/2} \partial_x \mu^{-1/2} & 0 \end{bmatrix}, \quad (35)$$

and the transformed wave field vector is identified as $|\phi\rangle = \mathcal{T}[\tilde{u}, \tilde{v}]^T$. This leads to a continuous Schrödinger equation

$$i\partial_t |\phi(t)\rangle = \mathcal{H} |\phi(t)\rangle, \quad (36)$$

subject to the transformed initial conditions

$$|\Phi(0)\rangle = \mathcal{T} \begin{bmatrix} \rho^{1/2} u_0 \\ \rho^{1/2} v_0 \end{bmatrix}. \quad (37)$$

It is now possible to discretise the continuous Schrödinger equation directly by discretising $\mu^{1/2} \partial_x \rho^{-1/2}$ with any numerical method, provided that the boundary conditions can be satisfied.

5.4 Extensions

The work presented here is merely a first step towards QC wave simulations in geophysical applications. Generalising to higher space dimensions will require a similar procedure as above to map the augmented wave operator \mathcal{Q} or its discretised version \mathbf{Q} to the Hamiltonian operator, ensuring self-adjointness under the quantum inner product. A bigger challenge may be the incorporation of visco-elastic attenuation because HS inherently conserves energy.

6 CONCLUSIONS AND OUTLOOK

We presented a quantum computing concept for 1-D elastic wave propagation through heterogeneous media. Our approach involves (1) a finite-difference approximation of the wave equation, (2) a sparsity-preserving transformation to a Schrödinger equation, and (3) direct simulation of the Schrödinger equation on a gate-based quantum computer.

The implementation of our approach on an error-free quantum simulator, produces nearly exact results and serves as the foundation of wave field simulations with small numbers of grid points on the real quantum computer IBM Brisbane. While the simulation results qualitatively agree with the error-free version, they are contaminated by errors related to quantum decoherence and noise, which are typical issues for today's quantum computers.

A continuous version of the discrete transformation to the Schrödinger equation enables the modification of our method based on finite differences, including the use of other spatial discretisation schemes, such as the spectral-element method. Assuming that error-corrected quantum chips will become available, an analogy between our method and coupled mass-spring systems suggests that our quantum computing approach may lead to wave field simulations that run exponentially faster than simulations on classical computers. This perspective motivates ongoing research on the extension of the 1-D elastic case to 3-D scenarios that include visco-elastic attenuation.

ACKNOWLEDGMENTS

We would like to thank the other members of the ETH Seismology & Wave Physics Group for fruitful discussions and inspiration. All codes used in this work are available at <https://github.com/malteschade/Quantum-Wave-Equation-Solver>.

Data statement: No data have been used for this research.

Author contribution statement: theory and study conception: C. Bösch; implementation and execution on the quantum computer : M. Schade; quantum computing introduction: V. Hapla; analysis and interpretation of results: M. Schade, C. Bösch, V. Hapla, A. Fichtner; manuscript preparation: M. Schade, C. Bösch, V. Hapla, A. Fichtner. All authors review the results and approved the final version of the manuscript.

REFERENCES

Adedoyin, A., J. Ambrosiano, P. Anisimov, W. Casper, G. Chennupati, C. Coffrin, H. Djidjev, D. Gunter, S. Karra, and N. Lemons (2022). Quantum algorithm implementations for beginners. *ACM Transactions on Quantum Computing* 3(4), 18:1–18:92.

Al-Mohy, A. H. and N. J. Higham (2010). A new scaling and squaring algorithm for the matrix exponential. *SIAM Journal on Matrix Analysis and Applications* 31(3), 970–989.

Aleksandrowicz, G., T. Alexander, P. Barkoutsos, L. Bello, Y. Ben-Haim, D. Bucher, F. J. Cabrera-Hernández, J. Carballo-Franquis, A. Chen, C.-F. Chen, et al. (2019). Qiskit: An open-source framework for quantum computing.

Babbush, R., D. W. Berry, R. Kothari, R. D. Somma, and N. Wiebe (2023). Exponential quantum speedup in simulating coupled classical oscillators. *arXiv preprint arXiv:2303.13012*.

Benenti, G., G. Casati, and G. Strini (2004). *Principles of quantum computation and information-volume I: Basic concepts*. World scientific.

Berry, D. W., G. Ahokas, R. Cleve, and B. C. Sanders (2007). Efficient quantum algorithms for simulating sparse hamiltonians. *Communications in Mathematical Physics* 270, 359–371.

Berry, D. W., A. M. Childs, R. Cleve, R. Kothari, and R. D. Somma (2015). Simulating Hamiltonian dynamics with a truncated Taylor series. *Phys. Rev. Lett.* 114, 090502–1–090502–5.

Bozdag, E., D. Peter, M. Lefebvre, D. Komatitsch, J. Tromp, J. Hill, N. Podhorszki, and D. Pugmire (2016). Global adjoint tomography: First-generation model. *Geophys. J. Int.* 207, 1739–1766.

Bravyi, S., A. W. Cross, J. M. Gambetta, D. Maslov, P. Rall, and T. J. Yoder (2023). High-threshold and low-overhead fault-tolerant quantum memory. *arXiv preprint arXiv:2308.07915*.

Bulmer, J. F., B. A. Bell, R. S. Chadwick, A. E. Jones, D. Moise, A. Rigazzi, J. Thorbecke, U.-U. Haus, T. Van Vaerenbergh, and R. B. Patel (2022). The boundary for quantum advantage in gaussian boson sampling. *Science advances* 8(4), eabl9236.

Childs, A. M., D. Maslov, Y. Nam, N. J. Ross, and Y. Su (2018). Toward the first quantum simulation with quantum speedup. *Proceedings of the National Academy of Sciences* 115(38), 9456–9461.

Collins, H. and K. Easterly (2021). Ibm unveils breakthrough 127-qubit quantum processor. *IBM Newsroom*.

Costa, P. C., S. Jordan, and A. Ostrander (2019). Quantum algorithm for simulating the wave equation. *Physical Review A* 99(1), 012323.

Daley, A. J., I. Bloch, C. Kokail, S. Flannigan, N. Pearson, M. Troyer, and P. Zoller (2022). Practical quantum advantage in quantum simulation. *Nature* 607(7920), 667–676.

Dhand, I. and B. C. Sanders (2014). Stability of the Trotter–Suzuki decomposition. *Journal of Physics A: Mathematical and Theoretical* 47(26), 265206.

Dormand, J. R. and P. J. Prince (1980). A family of embedded runge-kutta formulae. *Journal of computational and applied mathematics* 6(1), 19–26.

França, D. S. and R. Garcia-Patron (2022). A game of quantum advantage: Linking verification and simulation. *Quantum* 6, 753.

Gambetta, J. (2020). Ibm’s roadmap for scaling quantum technology. *IBM Research Blog (September 2020)*.

Gebraad, L. and A. Fichtner (2023). Seamless GPU acceleration for C++-based physics with the Metal Shading Language on Apple’s M series unified chips. *Seismological Research Letters* 94(3), 1670–1675.

Georgescu, I. M., S. Ashhab, and F. Nori (2014). Quantum simulation. *Reviews of Modern Physics* 86(1), 153.

Gibney, E. (2019). Hello quantum world! google publishes landmark quantum supremacy claim. *Nature* 574(7779), 461–463.

Gleinig, N. and T. Hoefer (2021). An efficient algorithm for sparse quantum state preparation. In *Proceedings: 58th Design Automation Conference*, pp. 433–438. IEEG.

Grover, L. K. (1996). A fast quantum mechanical algorithm for database search. In *Proceedings of the twenty-eighth annual ACM symposium on Theory of computing*, pp. 212–219.

Gyurik, C., C. Cade, and V. Dunjko (2022). Towards quantum advantage via topological data analysis. *Quantum* 6, 855.

Harrow, A. W., A. Hassidim, and S. Lloyd (2009). Quantum algorithm for linear systems of equations. *Physical review letters* 103(15), 150502.

Hatano, N. and M. Suzuki (2005). *Finding exponential product formulas of higher orders*, pp. 37–68. Springer.

Hibat-Allah, M., M. Mauri, J. Carrasquilla, and A. Perdomo-Ortiz (2023). A framework for demonstrating practical quantum advantage: Racing quantum against classical generative models.

Huang, H.-Y., M. Broughton, J. Cotler, S. Chen, J. Li, M. Mohseni, H. Neven, R. Babbush, R. Kueng, and J. Preskill (2022). Quantum advantage in learning from experiments. *Science* 376(6598), 1182–1186.

Igel, H., H. Djikpesse, and A. Tarantola (1996). Waveform inversion of marine reflection seismograms for P impedance and Poisson’s ratio. *Geophys. J. Int.* 124, 363–371.

Igel, H., P. Mora, and B. Riollet (1995). Anisotropic wave propagation through FD grids. *Geophysics* 60, 1203–1216.

Jin, S., N. Liu, and C. Ma (2023). Quantum simulation of maxwell’s equations via schrödingerisation. *arXiv preprint arXiv:2308.08408*.

Jin, S., N. Liu, and Y. Yu (2022). Quantum simulation of partial differential equations via schrodingerisation: Technical details. *arXiv preprint arXiv:2212.14703*.

Kak, S. (1999). The initialization problem in quantum computing. *Foundations of Physics* 29, 267–279.

Kane, C. L. and T. C. Lubensky (2014). Topological boundary modes in isostatic lattices. *Nature Physics* 10(1), 39–45.

Kim, Y., A. Eddins, S. Anand, K. X. Wei, E. Van Den Berg, S. Rosenblatt, H. Nayfeh, Y. Wu, M. Zaletel, K. Temme, et al. (2023). Evidence for the utility of quantum computing before fault tolerance. *Nature* 618(7965), 500–505.

Knill, E. (2005). Quantum computing with realistically noisy devices. *Nature* 434(7029), 39–44.

Liu, Y., S. Arunachalam, and K. Temme (2021). A rigorous and robust quantum speed-up in supervised machine learning. *Nature Physics* 17(9), 1013–1017.

Liu, Y., X. Liu, F. Li, H. Fu, Y. Yang, J. Song, P. Zhao, Z. Wang, D. Peng, and H. Chen (2021). Closing the “quantum supremacy” gap: Achieving real-time simulation of a random quantum circuit using a new sunway supercomputer. In *Proceedings of the International Conference for High Performance Computing, Networking, Storage and Analysis, SC ’21*, New York, NY, USA, pp. 1–12. Association for Computing Machinery.

Low, G. H. and I. L. Chuang (2019). Hamiltonian simulation by qubitization. *Quantum* 3, 163.

Madsen, L. S., F. Laudenbach, M. F. Askarani, F. Rortais, T. Vincent, J. F. Bulmer, F. M. Miatto, L. Neuhaus, L. G. Helt, and M. J. Collins (2022). Quantum computational advantage with a programmable photonic processor. *Nature* 606(7912), 75–81.

Maslov, D., J.-S. Kim, S. Bravyi, T. J. Yoder, and S. Sheldon (2021). Quantum advantage for computations with limited space. *Nature Physics* 17(8), 894–897.

Moczo, P., J. Kristek, and M. Gális (2014). *The finite-difference modelling of earthquake motions: Waves and ruptures*. CUP.

Montanaro, A. (2016). Quantum algorithms: An overview. *npj Quantum Information* 2(1), 1–8.

Moradi, S., D. Trad, and K. A. Innanen (2018). Quantum computing in geophysics: Algorithms, computational costs, and future applications. In *SEG International Exposition and Annual Meeting*, pp. SEG–2018. SEG.

Moradi, S., D. Trad, and K. A. Innanen (2019, 12). When quantum computers arrive on seismology’s doorstep. *Canadian Journal of Exploration Geophysics* 44, 1–20.

Nielsen, M. A. and I. L. Chuang (2010). *Quantum computation and quantum information*. CUP.

Preskill, J. (2018). Quantum computing in the nisq era and beyond. *Quantum* 2, 79.

Press, F. (1968). Earth models obtained by Monte-Carlo inversion. *J. Geophys. Res.* 73, 5223–5234.

Sanders, B. C. (2021). Quantum leap for quantum primacy. *Physics* 14, 147.

Sevilla, J. and C. J. Riedel (2020). Forecasting timelines of quantum computing. *arXiv preprint arXiv:2009.05045*.

Shampine, L. F. (1986). Some practical runge-kutta formulas. *Mathematics of Computation* 46(173), 135–150.

Shor, P. W. (1994). Algorithms for quantum computation: Discrete logarithms and factoring. In *Proceedings: 35th Annual Symposium on Foundations of Computer Science*, pp. 124–134. IEEG.

Shor, P. W. (1999). Polynomial-time algorithms for prime factorization and discrete logarithms on a quantum computer. *SIAM review* 41(2), 303–332.

Sivak, V., A. Eickbusch, B. Royer, S. Singh, I. Tsoutsios, S. Ganjam, A. Miano, B. Brock, A. Ding, and L. Frunzio (2023). Real-time quantum error correction beyond break-even. *Nature* 616(7955), 50–55.

Smolin, J. A., J. M. Gambetta, and G. Smith (2012). Efficient method for computing the maximum-likelihood quantum state from measurements with additive gaussian noise. *Physical review letters* 108(7), 070502.

Suau, A., G. Staffelbach, and H. Calandra (2021). Practical quantum computing: Solving the wave equation using a quantum approach. *ACM Transactions on Quantum Computing* 2(1), 1–35.

Süsstrunk, R. and S. D. Huber (2016). Classification of topological phonons in linear mechanical metamaterials. *Proceedings of the National Academy of Sciences* 113(33), E4767–E4775.

Suzuki, M. (1976). Generalized trotter’s formula and systematic approximants of exponential operators and inner derivations with applications to many-body problems. *Communications in Mathematical Physics* 51(2), 183–190.

Suzuki, M. (1991). General theory of fractal path integrals with applications to many-body theories and statistical physics. *Journal of Mathematical Physics* 32(2), 400–407.

Trotter, H. F. (1959). On the product of semi-groups of operators. *Proceedings of the American Mathematical Society* 10(4), 545–551.

Watrous, J. (2018). *The theory of quantum information*. CUP.

Yi, C. and E. Crosson (2022). Spectral analysis of product formulas for quantum simulation. *npj Quantum Information* 8(1), 1–6.

Zhang, X.-M. and X. Yuan (2023). On circuit complexity of quantum access models for encoding classical data. *arXiv preprint arXiv:2311.11365*.

APPENDIX A: CONTINUOUS TRANSFORMATION

Here, we construct an invertible transformation \mathcal{T} that transforms the continuous 1-D elastic wave equation to a continuous Schrödinger equation. We consider functions $a(x)$ that are differentiable at least once and satisfy either $a(0) = f(W) = 0$, $a(0) = 0$ and $\partial_x a(W) = 0$, or $\partial_x a(0) = 0$ and $a(W) = 0$, which define three different Hilbert spaces $\mathbb{H}_{D,D}$, $\mathbb{H}_{D,N}$ or $\mathbb{H}_{N,D}$ referring to either two Dirichlet or at least one Dirichlet boundary condition. All three Hilbert spaces are equipped with the natural inner product

$$\langle a, b \rangle = \int_0^W dx a^*(x)b(x), \quad a, b \in \mathbb{H}_{B,B'}, \quad (A1)$$

for $B, B' \in \{D, N\}$, and where $*$ denotes complex conjugation. We introduce the adjoint operator, \mathcal{A}^\dagger of some operator \mathcal{A} , corresponding to the above inner product and satisfying

$$\langle a, \mathcal{A}b \rangle = \langle \mathcal{A}^\dagger a, b \rangle, \quad a, b \in \mathbb{H}_{B,B'}. \quad (A2)$$

An operator, \mathcal{A} is self-adjoint, i.e. $\mathcal{A}^\dagger = \mathcal{A}$, if $\langle a, \mathcal{A}b \rangle = \langle \mathcal{A}a, b \rangle$, and anti-self-adjoint if $\langle a, \mathcal{A}b \rangle = -\langle \mathcal{A}a, b \rangle$, i.e. $\mathcal{A}^\dagger = -\mathcal{A}$. For two operators \mathcal{A} and \mathcal{B} we have that $(\mathcal{A}\mathcal{B})^\dagger = \mathcal{B}^\dagger\mathcal{A}^\dagger$. Furthermore, in $\mathbb{H}_{D,D}$, $\mathbb{H}_{D,N}$ and $\mathbb{H}_{N,D}$ we have $\partial_x^\dagger = -\partial_x$, which can be established through integration by parts and invoking the boundary conditions. With these properties of the adjoint operator we can express the mass-transformed wave operator as

$$\mathcal{L}_\rho := \rho^{-1/2} \partial_x [\mu \partial_x] \rho^{-1/2} = -[\mu^{1/2} \partial_x \rho^{-1/2}]^\dagger \mu^{1/2} \partial_x \rho^{-1/2}. \quad (A3)$$

The differentiation operator ∂_x has inverses given by the indefinite integral $\int dx : f(x) \rightarrow F(x) + C$, with a constant C and $\partial_x F(x) = f(x)$. Assuming at least one Dirichlet boundary, which results in the Hilbert spaces considered here, any wave field has zero offset $C = 0$, rendering the inverse unique. We can, therefore, construct

$$\mathcal{T} := \begin{bmatrix} \mu^{1/2} \partial_x \rho^{-1/2} & 0 \\ 0 & 1 \end{bmatrix}, \quad (A4)$$

with its right inverse given by

$$\mathcal{T}^{-1} = \begin{bmatrix} \rho^{1/2} \int dx \mu^{-1/2} & 0 \\ 0 & 1 \end{bmatrix}. \quad (A5)$$

This leads to

$$\mathcal{T} \mathcal{Q} \mathcal{T}^{-1} = \mathcal{T} \begin{bmatrix} 0 & 1 \\ \mathcal{L}_\rho & 0 \end{bmatrix} \mathcal{T}^{-1} = \begin{bmatrix} 0 & \mu^{1/2} \partial_x \rho^{-1/2} \\ -[\mu^{1/2} \partial_x \rho^{-1/2}]^\dagger & 0 \end{bmatrix} = \begin{bmatrix} 0 & \mu^{1/2} \partial_x \rho^{-1/2} \\ \rho^{1/2} \partial_x \mu^{-1/2} & 0 \end{bmatrix}, \quad (A6)$$

which is clearly anti-self-adjoint under the quantum inner product (34) of the quantum Hilbert space, $\mathbb{H}^q = \mathbb{H}_{B,B'} \oplus \mathbb{H}_{B,B'}$. Finally, we conclude that $H = i\mathcal{T} \mathcal{Q} \mathcal{T}^{-1}$ is therefore self-adjoint.

APPENDIX B: COMPLEXITY OF SPARSE HAMILTONIAN SIMULATION

To apply the Hamiltonian simulation approach from section 2.3, the quantum circuit needs to be properly initialised per (28). Today’s best sparse state initialisation methods need $\mathcal{O}(nS^2 \log(S))$ classical operations, producing a circuit with $\mathcal{O}(nS)$ quantum gates, where n is the qubit count and S is the number of non-zero initial conditions (Gleini and Hoefer, 2021). This cost can be amortised with relative ease if $S \ll 2^n$, which matches typical use cases.

To provide insight into the complexity of the time evolution itself using the currently best available methods, we first need to discuss the implementation of sparse matrices in general. Sparse matrices are typically implemented on QCs using oracles, which are functions that map one integer vector into another. A quantum oracle must be a unitary operation, and it can be shown that this requirement can be satisfied for any classical function by augmenting both its input and output with additional helper qubits appropriately. To represent a d -sparse matrix \mathbf{X} , two oracles are used: (1) one that takes a row index i and column index j , and returns the value $\mathbf{X}(i, j)$, and (2) one that takes a row index i and nonzero index $l \in [0, d)$, and returns the column index j of the l -th nonzero element in the row i .

As described in section 2.3, the action of the time-evolution operator $e^{-i\mathbf{H}t}$ is carried out only approximately because the exact matrix exponential evaluation is prohibitively expensive. There are multiple algorithms available that realise this approximation, the most efficient so far being HS by qubitisation (Low and Chuang, 2019). The input d -sparse Hamiltonian \mathbf{H} can be provided using the two oracles from above. For the time t and error ε , the qubitisation algorithm needs $\mathcal{O}(dt\|\mathbf{H}\|_{\max} + \log(1/\varepsilon))$ queries to the oracles. Here, $\|\mathbf{H}\|_{\max}$ is the maximum absolute value of \mathbf{H} . The error ε is the desired fidelity of the time-evolution operator, more specifically, the maximum admissible $\|\mathbf{U}' - \mathbf{U}\|_2$, where $\mathbf{U} = e^{-it\mathbf{H}}$ denotes the exact time-evolution operator, and \mathbf{U}' denotes its approximation produced by the algorithm. While HS is an area of active research, the query complexity of this algorithm already reaches fundamental lower bounds in the \mathcal{O} -notation. In the presented 1-D case, $d = 2$, as we have a 2-sparse Hamiltonian, and

$$\|\mathbf{H}\|_{\max} = \|\mathbf{U}\|_{\max} = \|\mathbf{E}^{1/2} \mathbf{DM}^{-1/2}\|_{\max} = \max_{i=0}^{2^n-1} \sqrt{\frac{\mu(x_i)}{\rho(x_i)}}.$$

Hence, the query complexity is linear in $d, t, \|\mathbf{H}\|_{\max}$ and $1/\varepsilon$. Assuming that ε, d and \mathbf{H}_{\max} do not depend on n , which clearly holds in our case here, the query complexity is constant in n , i.e., does not depend on the matrix size. It is usually assumed that the oracles themselves can be implemented with the polynomial runtime complexity, i.e., the circuit depth D is in $\mathcal{O}(n^k)$, implying the complexity of the whole Hamiltonian simulation is polynomial in n as well. However, bounds on the runtime complexity of a query are an area of active research (Zhang and Yuan, 2023). A more technical, in-depth analysis of the sparse Hamiltonian simulation utilised for simulating coupled classical oscillators and proofs establishing exponential speedup against classical algorithms can be found in Babbush et al. (2023).

APPENDIX C: GENERAL BOUNDARY CONDITIONS

The derived Hamiltonian formulation based on the FD matrix (14) naturally results in Dirichlet and Neumann boundary conditions (BCs) on the right and left side of the domain, respectively. We now extend this approach to arbitrary BCs, with at least one Dirichlet BC to ensure negative definiteness of the stiffness matrix. To that end, we define the non-square first-order-accurate forward finite-difference matrix \mathbf{D} as

$$\mathbf{D} = \frac{1}{\Delta x} \begin{bmatrix} d_{\text{left}} & 0 & 0 & \dots & 0 \\ 1 & -1 & 0 & \dots & 0 \\ 0 & 1 & -1 & \dots & 0 \\ 0 & 0 & 1 & \dots & 0 \\ \vdots & \vdots & \vdots & \ddots & \vdots \\ 0 & 0 & 0 & \dots & 1 & -1 \\ 0 & 0 & 0 & \dots & 0 & d_{\text{right}} \end{bmatrix} \in \mathbb{R}^{2^{n-1} \times (2^{n-1}-1)}. \quad (\text{C1})$$

For Dirichlet-Dirichlet boundary conditions, $d_{\text{left}} = d_{\text{right}} = 1$. If one of the BCs is Neumann, then we set respectively $d_{\text{left}} = 0$ or $d_{\text{right}} = 0$. The symmetric negative-definite stiffness matrix \mathbf{K} is obtained as

$$\mathbf{K} = -\mathbf{D}^T \mathbf{E} \mathbf{D} \in \mathbb{R}^{(2^{n-1}-1) \times (2^{n-1}-1)}, \quad (\text{C2})$$

where $\mathbf{E} \in \mathbb{R}^{2^{n-1} \times 2^{n-1}}$. We obtain the mass-transformed stiffness matrix $\tilde{\mathbf{K}}$ as

$$\tilde{\mathbf{K}} = \mathbf{M}^{-1/2} \mathbf{K} \mathbf{M}^{-1/2} = -\mathbf{U}^T \mathbf{U} \in \mathbb{R}^{(2^{n-1}-1) \times (2^{n-1}-1)} \quad (\text{C3})$$

with $\mathbf{M}^{-1/2} \in \mathbb{R}^{(2^{n-1}-1) \times (2^{n-1}-1)}$, and consequently

$$\mathbf{U} = \mathbf{E}^{1/2} \mathbf{D} \mathbf{M}^{-1/2} \in \mathbb{R}^{2^{n-1} \times (2^{n-1}-1)}. \quad (\text{C4})$$

We can now define the transformation

$$\mathbf{T} = \begin{bmatrix} \mathbf{U} & \mathbf{0} \\ \mathbf{0} & \mathbb{1}_{2^{n-1} \times (2^{n-1}-1)} \end{bmatrix} \in \mathbb{R}^{2^n \times (2^{n-2})}, \quad (\text{C5})$$

which has full column rank and hence a unique left inverse \mathbf{T}^+ , i.e., $\mathbf{T}^+\mathbf{T} = \mathbf{I}$. With the impedance matrix \mathbf{Q} defined as

$$\mathbf{Q} = \begin{bmatrix} \mathbf{0} & \mathbb{1}_{(2^{n-1}-1) \times (2^{n-1}-1)} \\ \tilde{\mathbf{K}} & \mathbf{0} \end{bmatrix} \in \mathbb{R}^{(2^n-2) \times (2^n-2)}, \quad (\text{C6})$$

we finally obtain the Hermitian Hamiltonian $\mathbf{H} \in \mathbb{R}^{2^n \times 2^n}$ as

$$\mathbf{H} = i\mathbf{T}\mathbf{Q}\mathbf{T}^+ = i \begin{bmatrix} \mathbf{U} & \mathbf{0} \\ \mathbf{0} & \mathbb{1}_{2^{n-1} \times (2^{n-1}-1)} \end{bmatrix} \begin{bmatrix} \mathbf{0} & \mathbb{1}_{(2^{n-1}-1) \times (2^{n-1}-1)} \\ -\mathbf{U}^T \mathbf{U} & \mathbf{0} \end{bmatrix} \begin{bmatrix} \mathbf{U}^+ & \mathbf{0} \\ \mathbf{0} & \mathbb{1}_{(2^{n-1}-1) \times 2^{n-1}} \end{bmatrix}, \quad (\text{C7})$$

which we use in the Hamiltonian simulation. Note this formulation allows for $2^{n-1} - 1$ grid points for n qubits.